Min Zhang[1]
Laser Processing Research Center,
School of Mechanical and Electrical Engineering,
Soochow University,
Suzhou, Jiangsu 215021, China
e-mail: mzhang@aliyun.come

Chang Jun Chen
Laser Processing Research Center,
School of Mechanical and Electrical Engineering,
Soochow University,
Suzhou, Jiangsu 215021, China
e-mail: chjchen2001@aliyun.com

Grant Brandal
Advanced Manufacturing Laboratory,
Department of Mechanical Engineering,
Columbia University,
New York, NY 10027
e-mail: gbb2114@columbia.edu

Dakai Bian
Advanced Manufacturing Laboratory,
Department of Mechanical Engineering,
Columbia University,
New York, NY 10027
e-mail: db2875@columbia.edu

Y. Lawrence Yao
Advanced Manufacturing Laboratory,
Department of Mechanical Engineering,
Columbia University,
New York, NY 10027
e-mail: yly1@columbia.edu

Experimental and Numerical Investigation of Laser Forming of Closed-Cell Aluminum Foam

Aluminum foams are generally very attractive because of their ability of combining different properties such as strength, light weight, thermal, and acoustic insulation. These materials, however, are typically brittle under mechanical forming, and this severely limits their use. Recent studies have shown that laser forming is an effective way for foam panel forming. In this paper, the laser formability of Al–Si closed-cell foam through experiments and numerical simulations was investigated. The bending angle as a function of the number of passes at different laser power and scan velocity values was investigated for large- and small-pore foams. In the finite element analysis, both effective-property and cellular models were considered for the closed-cell foam. Multiscan laser forming was also carried out and simulated to study the accumulative effect on the final bending angle and stress states. The maximum von Mises stress in the scanning section was on the order of 0.8 MPa, which was lower than the yield strength of the closed-cell foam material. This paper further discussed the reasonableness and applicability of the two models. [DOI: 10.1115/1.4030511]

Keywords: Al–Si closed-cell foam, laser forming, finite element analysis, cellular model and effective-property model

1 Introduction

Metal foams are a new class of materials with low densities and novel physical, mechanical, thermal, electrical, and acoustic properties. They offer potential for lightweight structures, for energy absorption, and for thermal management. Aluminum foams are a typical example as aluminum foams combine good strength and stiffness with low weight and insulation properties. Aluminum foam can be used as structure and function materials. Structural applications include automotive bumper, aerospace section, ship building, and railway industry [1]. These materials, however, are typically brittle under mechanical forming and shaping, and this fact severely limits their structure application. Recent studies [2,3] have shown that laser forming is feasible for foam panel forming.

The feasibility of laser forming of aluminum foam sandwich (AFS) panels has been investigated by Guglielmotti et al. [2]. AFS panels consisted of two thin AA6082 cover sheets and a closed-cell foam core made of Al–Si–Mg. The effect of the main process parameters (laser power and scan velocity) on the bending efficiency of various panel thicknesses was investigated as well as the contribution of the panel skin and the protective gas. A good formability was observed for the laser processed panels and very high bending angles were reached with a proper combination of the process parameters. More recently, this study has been extended to open-cell Al foams by Quadrini et al. [3]. Different densities of AlSi7Mg open-cell foam aluminum and the effect of the main process parameters on the bending efficiency were investigated. Experimental results showed that the bending angle of open-cell aluminum foam [3] is quite different from closed-cell aluminum foam [2] under the same laser parameters. According to the theory of Coquard and Baillis [4], the difference has been attributed to the fact that thermal conductivity and other factors for open and closed-cell foam aluminum are different.

The process window determination of laser forming is quite complex as many geometrical and process parameters have to be considered; moreover, the process window is very narrow and it is very easy to produce foam degradation during forming. The numerical approach is often beneficial to help investigate optimal process conditions as a function of the process variables and the material properties and geometry. More recently, a 3D thermomechanical model was developed to study the mechanical and laser bending of open-cell aluminum foam [5,6]. In numerical simulations [5] performed in 2010, a bilinear isotropic hardening was assumed to simulate the material behavior during plastic deformation. Only a small domain of the foam was modeled so as to reduce computational time; simulation results show that the temperature gradient mechanism (TGM) is active in the laser forming of open-cell Al foams but the homogeneity of temperature and stress maps is affected by the nonhomogeneity of the foam structure. In 2013, mechanical and laser bendings of a large sample are simulated for the first time by Quadrini et al. [6] with the same simulation method as in Ref. [5], results showed the shape evolution and temperature/displacement history at some critical locations during laser forming. No comparison, however, was made between simulation and experimental results.

In this paper, two different geometrical models are proposed for the closed-cell foam aluminum. Thermal, mechanical, and multiscans laser bending of closed-cell aluminum foam are simulated

[1]Corresponding author.

Contributed by the Manufacturing Engineering Division of ASME for publication in the Journal of Manufacturing Science and Engineering. Manuscript received December 17, 2014; final manuscript received April 1, 2015; published online September 9, 2015. Assoc. Editor: Hongqiang Chen.

and analyzed in detail to elucidate laser forming mechanisms of closed-cell foam aluminum. The simulation results were compared with experimental results for the first time and the reasonableness of two simulation models was investigated. Different plate thickness and pore size of close-cell aluminum beam are also studied.

2 Experimental Procedure

The closed-cell foam aluminum samples were manufactured with Al–7%Si eutectic alloy by the melting foaming method. The porosity of the closed-cell aluminum is 74–78%. The length of the samples is 100 mm, the width is 35 mm, and the thickness is 11 mm. Large size pores range 5–7 mm (Fig. 1(*a*)), and small size pores 3–5 mm (Fig. 1(*b*)). Their density is about 600 and 680 kg/m^3, respectively. The laser system used for laser forming experiments was a GSI-Lumonics laser and a Staubli RX1300 robot system. The maximum power of the laser was 2000 W and its wavelength was 1064 nm. A defocused beam diameter 8 mm was delivered via optical fiber and used. The samples were scanned by the movement of robot system. Typical processing parameters are laser beam power of 360 W and 400 W at a scanning speed of $V = 1.8$ and 2.4 mm/s. Passes of 70–100 were performed on each specimen, in sets of ten consecutive passes. After each set, the foam aluminum was left to cool in air for 5 min and the bending angle was evaluated by measuring the vertical displacement of the specimen free end in the middle width by means of a dial indicator. During laser scanning, a flow of protective gas (nitrogen) was provided on the processed zone so as to reduce oxidation at elevated temperature.

During bending, the laser beam was focused on the upper side of the specimen, the sheet was clamped on a robot motion table along the 35 mm edge. The specimens were scanned in the middle of the plate by moving them in a single direction under the motionless laser source. Each laser scan was 80 mm long, i.e., 45 mm longer than the specimen width to assure that the laser power was constant during the bending process.

3 Mathematical Analysis

3.1 Modeling of Laser Forming. The earlier work on laser forming of sheet metal began in the 1980 s including space application [7], and analytical models were subsequently developed [8]. The numerical approach is often more beneficial due to the complexity involved in the laser forming process. The effect of different processing parameters and different thermal boundaries on laser forming was studied [9–11]. Cheng and Yao numerically investigated cooling effects [12] in multiscan laser forming and size effect [13] of laser forming. Bao and Yao investigated edge effect [14] of laser forming. Li and Yao investigated the laser bending of tubes [15] and strain-rate effect [16] in laser forming. Shen and Vollertsen [17] have summarized developments in modeling of laser forming, including analytical models, numerical simulations, and empirical models. These researches mainly focus on laser forming of sheet metals and provide good starting points to laser forming of foam materials.

Laser forming of foam materials is more complex to model due to its cellular geometry and different properties. Foam consists of pores and the energy equation pertinent to laser forming needs to be modified to incorporate the presence of pores in the workpiece. A simplification is to use the continuum conservation equations to model the material as if it is solid and employs effective properties derived from those of closed-cell foam materials. This approach was taken in modeling foam in laser cutting [18] and lotus-type porous magnesium in laser welding [19]. Quadrini et al. [6] explicitly modeled the cellular structure of foam and assumed a bilinear isotropic hardening to simulate the material behavior during plastic deformation in laser forming of open-cell foam aluminum but the model was not validated using experimental results.

In this paper, we investigated two types of models: effective-property and cellular models. In the effective-property model, an aluminum foam plate is modeled as homogenous solid without cells, while material properties of aluminum foam are used. In the cellular model, the cellular structure is explicitly modeled, while properties of solid aluminum are used. The former is simpler but may not capture the crushable behavior of foams well. For laser forming applications, however, the level of compressive stress resulted from laser scanning may not reach the critical value of crush so the model is likely to be adequate. The latter is obviously more realistic because of the complex geometry, all cell structures are free meshed and final number of nodes could increase significantly.

Analysis of the numerical results [4] shows that the fraction of solid phase in the struts and vertices (lumps) of cells is the key structural characteristics. The shape of the cells and the shape of the cross sections of the struts have a weaker influence on the conductive heat transfer. For open-cell foams, when the lumps of solid phase are ignored, the structure modeled is close to regular open-cell without lumps, the effective thermal conductivity predicted is noticeably different from that computed numerically [4]. So for open-cell foam aluminium, the effective properties cannot be used in the thermal model of laser forming.

Fig. 1 (*a*) Large pore (pore size: 5–10 mm and average pore size: 7 mm) and (*b*) small pore (pore size: 3–5 mm) closed-cell foam aluminum (100 mm × 35 mm × 11 mm)

3.2 Thermal Modules. According to Refs. [4,19], if a realistic value of the fraction of foam in struts could be estimated, an empirical relation would provide an accurate prediction of the effective thermal conductivity of closed-cell foam. Hence, the first model is used in present paper with the assumption of effective properties resembling aluminum foam in laser forming closed-cell foam aluminum (Fig. 2(*a*)).

As the shape of the cells and the shape of the cross sections of the struts have a weaker influence on the conductive heat transfer [4], the cellular model used an elementary spherical feature as the cell (Fig. 2(*b*)). The cells are so placed that the density and porosity of the cellular model are similar to the mean density and porosity of the experimental foam aluminum.

In the thermal analysis of the laser forming of foam aluminum plate, the following assumptions are made:

(1) The thermal properties are isotropic; (2) The laser intensity distribution is in Gaussian mode; (3) Fourier heat conduction in the specimen and free convection and thermal radiation in the surrounding air are considered; (4) No melting during laser foaming of foam aluminum; and (5) The heat due to the strain energy is neglected so the thermal module is sequentially coupled with the mechanical module.

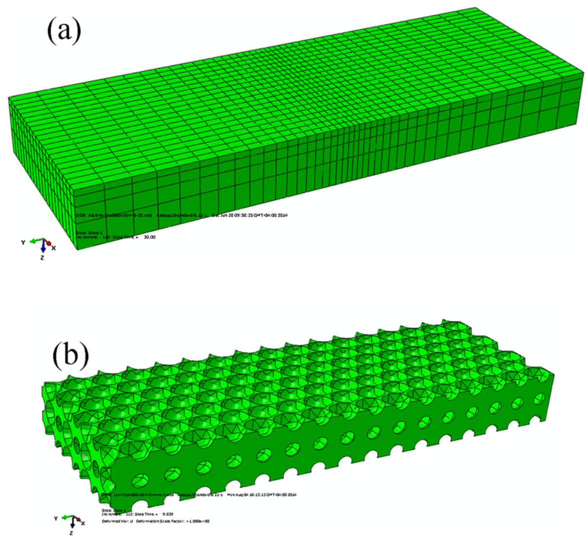

Fig. 2 Meshed geometry of (*a*) effective-property model and (*b*) cellular model (cell size = 7 mm) (100 mm × 35 mm × 11 mm)

In both thermal and mechanical modules, laser scanning plane is *X*–*Y* plane. In this plane, $Z = 0$ and laser scanning direction is *X*-direction, the bottom surface of specimen is in the positive direction of *Z*.

3.3 Stress Analysis. For the cellular model, the crushable foam model based on Deshpande and Fleck [20] is adopted. The model is primarily based on the experimental tests of aluminum foam and assumes similar behaviors in tension and compression, hence, isotropic hardening. This model has the simplest expression and has found widespread applications [19]. It is briefly summarized below.

The flow potential for the isotropic hardending model is chosen as

$$G = \sqrt{q^2 + \beta^2 p^2} \tag{1}$$

where β represents the shape of the flow potential and is

$$\beta = \frac{3}{\sqrt{2}}\sqrt{\frac{1 - 2v_p}{1 + v_p}} \tag{2}$$

where q is the von Mises equivalent stress, and p is the mean stress. v_p is the plastic Poisson's ratio given by

$$v_p = \frac{3 - k_2}{6} \tag{3}$$

where k_2 is the ratio of initial yield stress in uniaxial compression and initial yield stress in hydrostatic compression. The plastic strain rates are

$$\dot{\varepsilon}^{pl} = \dot{\lambda}\frac{\partial G}{\partial \sigma} \tag{4}$$

The plastic strain $\dot{\varepsilon}^{pl}$ is defined to be normal to a family of self-similar flow potential parameterized by the value of the potential β. Where $\dot{\lambda}$ is the non-negative plastic flow multiplier.

In both mechanical models, specimen is clamped at one end, where the displacement of *X*, *Y*, and *Z* directions is fully constrained.

3.4 Numerical Schemes. The above thermal and mechanical models are implemented in ABAQUS/standard. In the effective-property model, the 20-node element DC3D20 is used in the thermal and mechanical model. In order to capture high gradients near the scanning path, finer mesh is used in that region, while coarser mesh is employed in remote areas.

In the cellular model, the eight-node element DC3D8 and continuum stress/displacement elements with the same dimension and number of nodes DC3D8 are used for the thermal and mechanical analyses, respectively.

For both models, a user-defined subroutine is developed using FORTRAN to define the magnitude of the heat flux generated by the laser beam for top surface, which depends on the coupled laser power, beam diameter, scanning speed, and scanning scheme. Temperature and strain-rate dependent material properties were compiled and considered in the numerical models.

4 Results and Discussion

4.1 Experimental Results. Figure 3 shows a typical laser bent Al–Si foam plate after 40 scans. Figure 4 shows the bending angle as a function of the number of passes at different laser power and scan velocity values, for large- and small-pore foams. As expected, the bending angle increases with the increasing laser power and decreases with the increasing scan velocity. Within the power and velocity range used, the bending angle increases more or less linearly with the number of scans. Comparing Figs. 4(*a*) and 4(*b*), it is noted that higher bending angles were obtained for the low-density foam (large pores). This is due to a number of factors but chiefly due to the fact that more material is available near the bottom surface to resist laser-induced bending for the high density foam (small pores). This factor overwrites the fact that more material is thermally expanded and therefore plastically compressed near the top surface for the same foam. These experimental results were consistent with laser forming experiment results of open-cell aluminum plates and aluminum foam sandwiched (AFS) panels [2,3].

For some curves shown in Fig. 4, there is an abrupt increase in slope, as indicated by arrows. This happens after 30–40 laser scans under the condition of laser power of 360 W and scanning velocity of $V = 1.8$ mm/s and $V = 2.4$ mm/s of large pore and laser power of 420 W and scanning velocity of $V = 1.8$ mm/s of small pore. This is due to the formation of a crack at the bottom surface, as seen and shown in Fig. 5 after 40 laser scans under the condition of laser power of 360 W and scanning velocity of $V = 1.8$ mm/s. This clearly indicates that process optimization is crucial to avoid fracture from happening and will be investigated and explained with the following numerical results. Under all conditions, no crush of the foam structure was observed.

4.2 Numerical Model Validation. The effective-property model is compared with experimental results, as shown in Fig. 6. As it will be discussed in Sec. 4.5, the effective-property model works adequately for the conditions considered in this paper, while the cellular model offers some advantages. As a result, most

Fig. 3 Laser bent samples of large-pore closed-cell foam aluminum after 40 scans (laser powder = 360 W, scanning speed = 1.8 mm/s, and beam diameter = 8 mm)

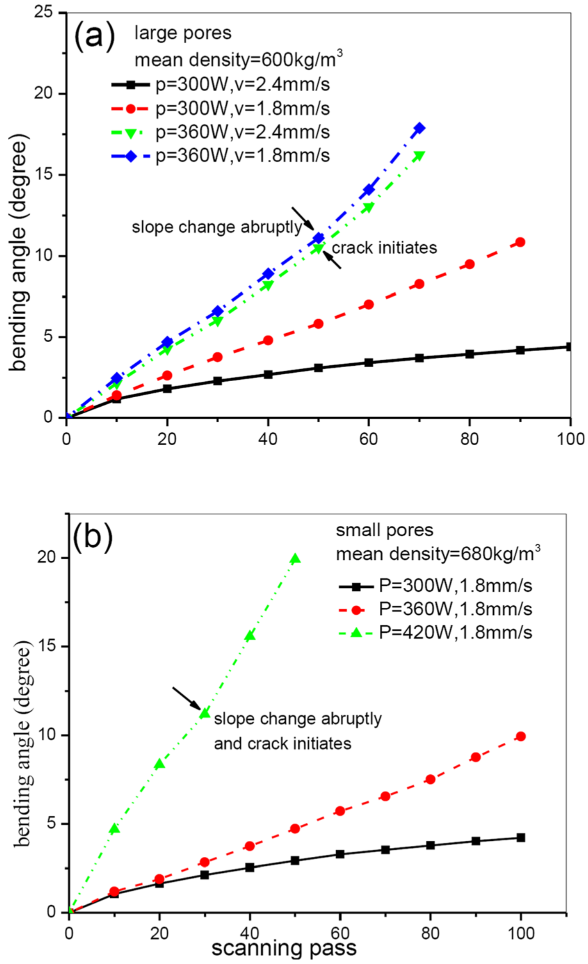

Fig. 4 Bending angle versus number of laser scans under different processing parameters: (*a*) large-pore and (*b*) small-pore foam aluminum plates

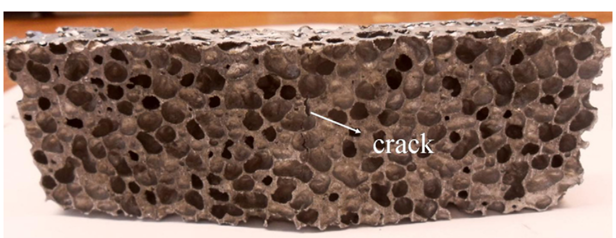

Fig. 5 Laser bent samples with crack formed at bottom surface after 40 scans (laser powder = 360 W, scanning speed = 1.8 mm/s, and beam diameter = 8 mm)

comparisons and analyses are based on the effective-property model. The comparison is made at the tenth scan, as the experimental procedure measures the bending angle after a set of ten scans only. The curved lines represent the numerical results which show the accumulative bending angle after ten scans. The numerical model generally agrees with experimental results. This helps establish the confidence on the numerical model. Under the condition of power of 360 W and velocity of 1.8 mm/s, the numerical result underestimates the experimental result. Note among the four conditions, this represents the highest energy input as the power is higher and the scanning speed is lower.

4.3 Analysis of Thermal Results. For laser forming of Al–Si closed-cell foam, a typical temperature history at the center of the laser impinging zone is shown in Fig. 7. It can be seen that the scanned region of the specimen has a large gradient in the thickness direction. So the TGM [8] is easier to establish in the foam materials. The temperature difference between top surface and middle surface is larger as compared with laser forming of homogeneous sheet metal. This is mainly caused by the lower thermal conductivity of the close-cell foam aluminum. In fact, in this way, low-density foam aluminum has thermal protection and insulation functions.

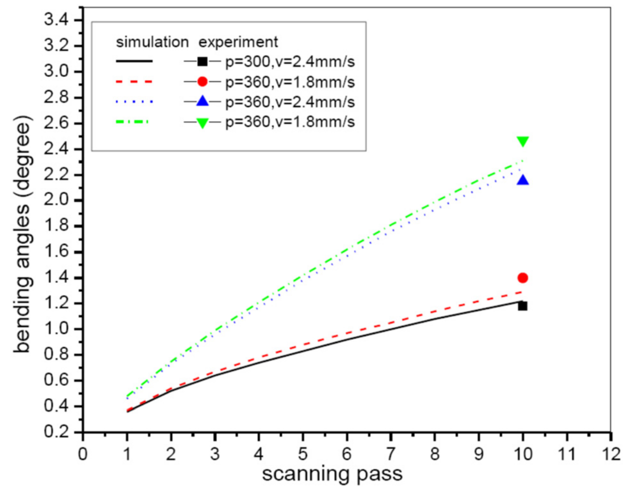

Fig. 6 Comparison of numerical (effective-property model) and experimental results of the large-pore foam laser bending angle (power: 300 W and 360 W, scanning speed: 1.8 and 2.4 mm/s, and beam diameter: 8 mm)

4.4 Analysis of Strain and Stress Field. The time history of the plastic strain developed after a single laser scan at the center of the laser scanning path is shown in Fig. 8. The depicted plastic strain is along the *y*-direction, that is, the direction perpendicular to the scan path and on the top surface.

At top surface, the conversion of thermal expansion into significant plastic compressive strain is seen. The compressive plastic strain recovers a little during cooling on the top surface primarily due to cooling-induced material contraction. In the bottom surface due to little temperature rise (Fig. 6) and therefore insignificant thermal expansion and compression, little plastic strain occurs.

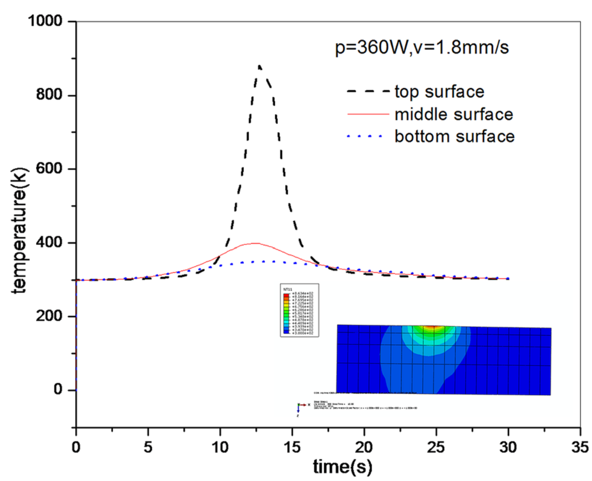

Fig. 7 Time history of temperature at the top/middle/bottom surface along the laser scanning path of large-pore foam aluminium (effective-property model)

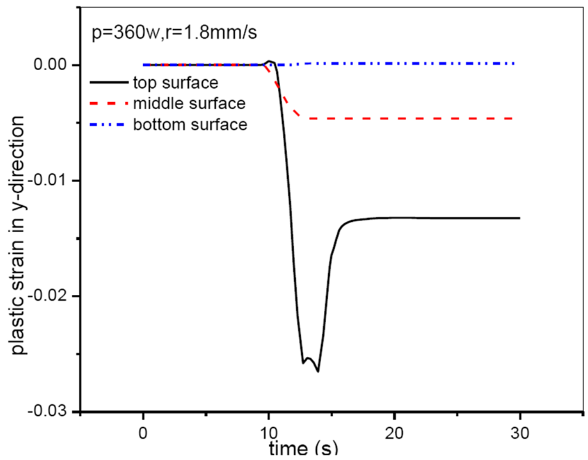

Fig. 8 Time history of plastic strain in *y*-direction (perpendicular to the scan direction on the top surface) along the laser scanning path of large-pore foam aluminum (effective-property model)

This pattern is similar to that seen in laser forming of homogeneous materials.

Figure 9 shows the *y*-direction stress history during a single scan laser scanning process. The location is again at the center of the laser scanning path. Compared to strain variation, the stress variation is more complex. Of particular interest is the tensile stress developed at the bottom surface, which reaches about 0.75 MPa at the end of the scan, which is comparable to what was reported in Ref. [21]. This level of stress is significantly below the fracture stress of the foam material but is from a single scan. The temperature rise at the bottom surface is very small (about 50 deg as seen from Fig. 7), so its stress change was mainly effected by bending of the plate.

To study the accumulative effects of multiscan laser forming, Fig. 10 shows the *y*-direction plastic strain/stress history at top/bottom surfaces during ten-pass laser scanning process. During the consecutive ten passes, an almost liner increment of plastic compressive strain at the topic surface is seen in Fig. 10(*a*). The total strain reaches about 0.13. This is consistent with the near-linear increment of bending angle as seen from Figs. 4 and 6. An almost linear increment in plastic tensile strain can be found in Fig. 10(*b*). The total strain is much smaller and in the order of 4.2×10^{-3}. This is consistent with the bent geometry of a plate. The stress at the bottom surface, however, levels off after the first few scans and reaches only about 1.25 MPa after ten scans, while the first scan generates about 0.75 MPa as discussed before. It is because the relaxation provided by the plastic tensile stress prevents stress from building up. This appears to be against the fact that a crack was observed at the bottom surface after 40 scans. But considering the fact that the strain at the bottom could reach about 17×10^{-3} after 40 scans if the pattern of linear increment holds, the fracture strain could be reached. As seen from the experimental stress/stress curves in Fig. 11 [21], the fracture strain

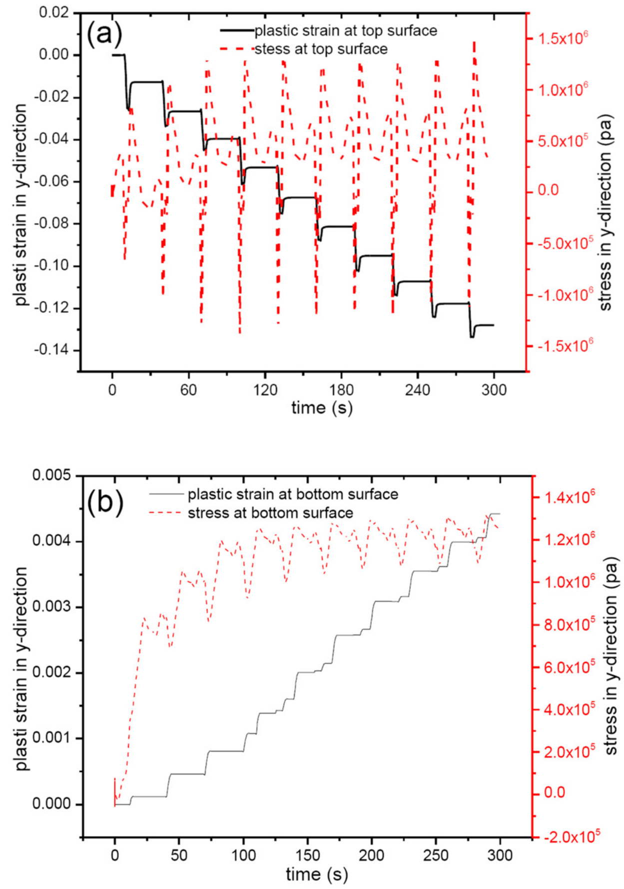

Fig. 10 Plastic strain/stress history in *y*-direction at (*a*) top surface and (*b*) bottom surface along the laser scanning path of ten-pass scanning of large-pore foam aluminum (effective-property model) (laser powder = 360 W, scanning speed = 1.8 mm/s, and beam diameter = 8 mm)

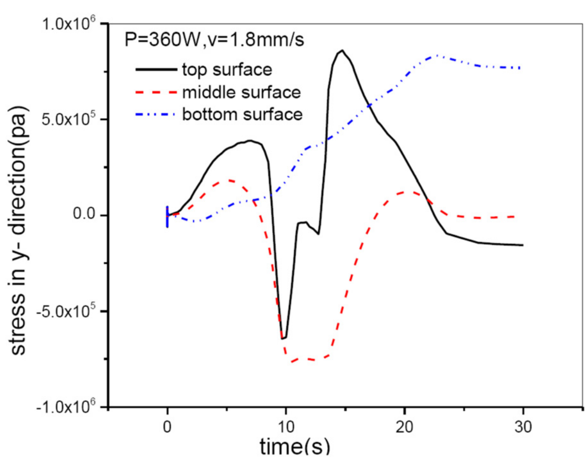

Fig. 9 Time history of stress in *y*-direction along the laser scanning path of large-pore foam aluminum (effective-property model)

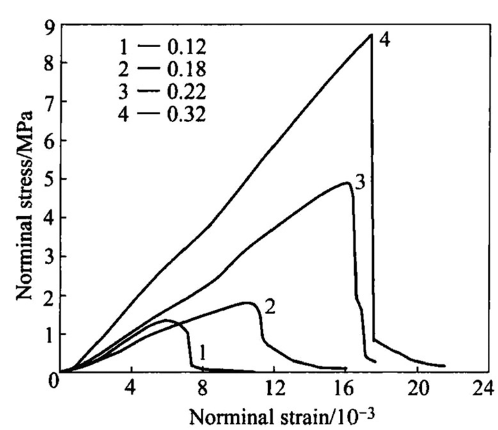

Fig. 11 Uniaxial tensile stress versus strain curves for Al–Si closed-cell aluminum foams with different relative densities [21]

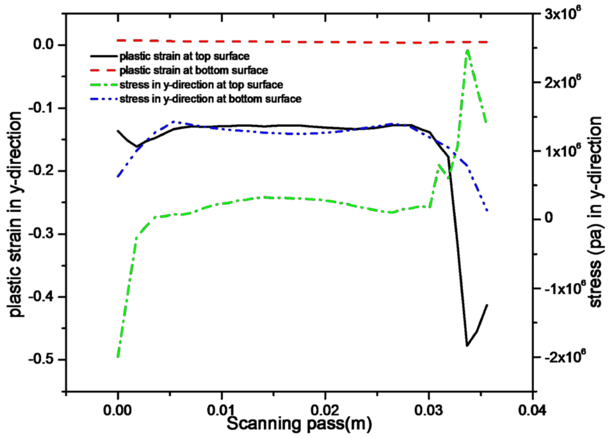

Fig. 12 Typical *Y*-direction plastic residual stress distribution along the scanning path after ten scans of large-pore foam aluminum (effective-property model) (laser powder = 360 W, scanning speed = 1.8 mm/s, and beam diameter = 8 mm)

is about 16×10^{-3} for Al–Si closed-cell aluminum foam with a relative density of 0.22. For the large-pore Al–Si foam used here, the relative density is about 0.22. Figure 12 also shows a plastic strain and residual stress distribution along the scanning path. As seen, some quantities at the ends differ significant from those at the middle of the plate due to the so-called edge effects [14].

4.5 Comparison of the Two Models. To compare the two models, a typical Al–Si closed-cell foam laser forming simulation is performed using both models. Figure 13 shows the temperature history at a typical point along the scanning path. Both models predict a similar temperature at the top surface while the effective-property model predicts a steeper temperature gradient along the thickness direction. This can also be seen by comparing the two temperature distribution color contours superposed in Fig. 13. As the effective-property model has been experimentally validated, it is reasonable to believe that the temperature gradient predicted by this model is more realistic. The cellular model, in which uniformly spaced spherical pores of the same diameter are used to approximate somewhat randomly spaced and sized pores in reality, gives less realistic prediction of temperature gradient.

As to the mechanical models, Fig. 14 qualitatively shows the bending results from the two models. The bending angle predicted by the cellular model is smaller than that predicted by the effective-property model likely due to the less steep temperature gradient in the thickness direction predicted by the cellular model. Figure 15 shows the temperature contour at the top surface and bottom surface. Figure 16 shows the y-direction plastic strain/stress history of a point on the top surface and bottom surface along the scanning path predicted by the cellular model. The points chosen are in the cell wall, edge of cell strut, and middle of cell strut, respectively. As seen in Fig. 16(*a*), at the top surface the plastic strain reaches a negative value at cell wall and cell strut middle, similar to that predicted by the effective-property model (Fig. 8), but there are two differences. It exhibits no plastic recovers during cooling compared with the effective-property model (Fig. 8). This is due to the fact that thermal insulation flow stress of heated material is slightly lower than its surrounding material. Another difference is plastic strain that reaches a positive value at cell strut edge, contrary to that predicted by the effective-property model (Fig. 7), this is due to the geometry size effect of foam aluminum [22], the strut edge can be considered as a very thin (100 μm) beam, so when thermal expansion occurred it will become permanent plastic deformation. As to the stress, Fig. 16(*a*) shows a similar pattern as that predicted by the effective-property model (Fig. 9) but the magnitude of the residue value of about $-(2.1–3) \times 10^6$ Pa is much larger than that predicted

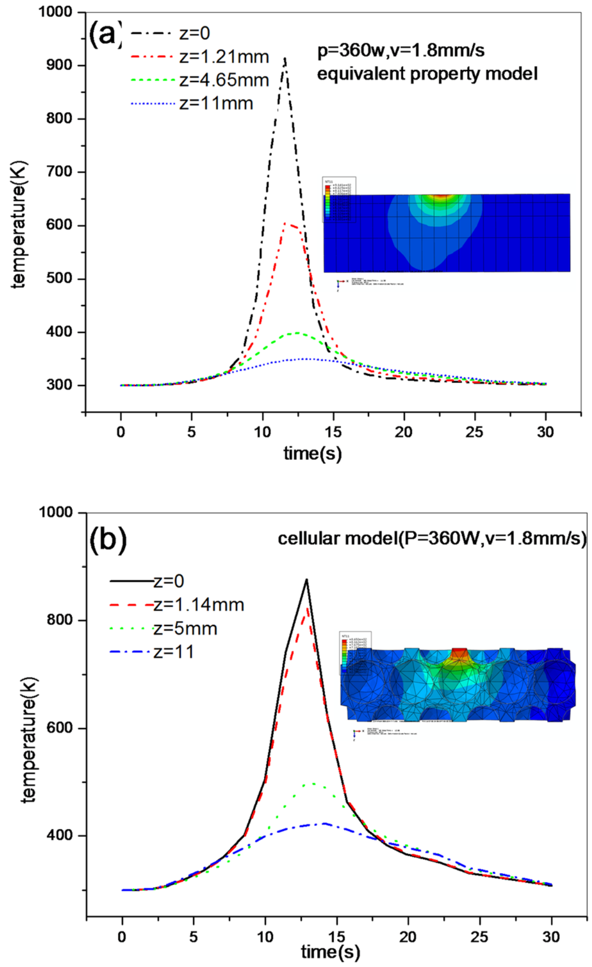

Fig. 13 Temperature history of typical point in (*a*) effective-property model and (*b*) cellular model (cell size = 7 mm) during laser scanning large pore foam aluminums with thickness of 11 mm (laser powder = 360 W, scanning speed = 1.8 mm/s, and beam diameter = 8 mm)

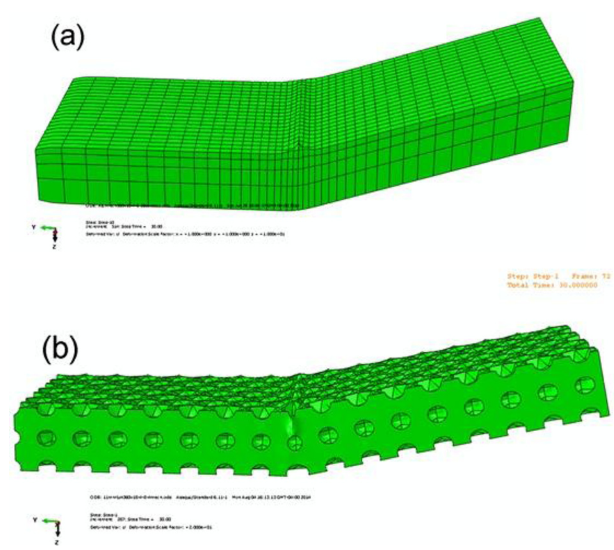

Fig. 14 Bending results of (*a*) effective-property model and (*b*) cellular model (cell size = 7 mm) after laser scanning of large-pore foam aluminum (laser powder = 360 W, scanning speed = 1.8 mm/s, and beam diameter = 8 mm, magnification 20 × for viewing clarity)

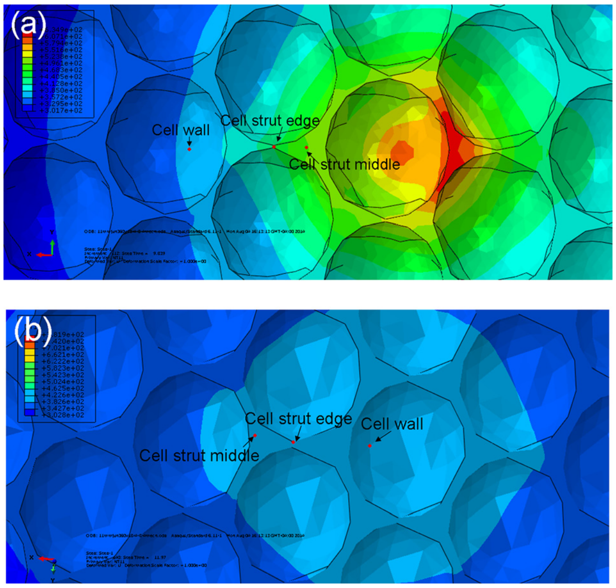

Fig. 15 Temperature contour at (*a*) top and (*b*) bottom surface of aluminum foam as predicated by the cellular model (cell size 7 mm) showing cell strut middle, cell strut edge, and cell wall. The laser scan is horizontally from right to left (laser powder = 360 W, scanning speed = 1.8 mm/s, and beam diameter = 8 mm).

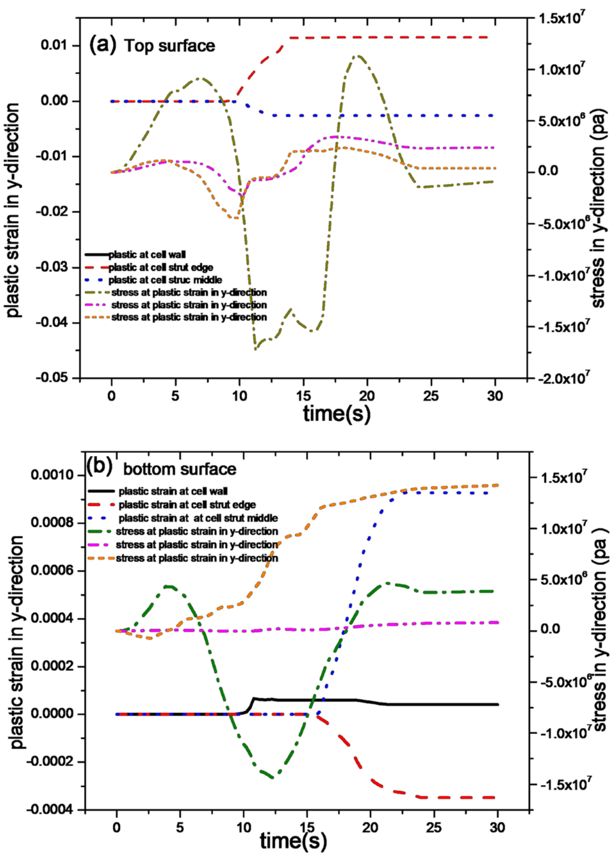

Fig. 16 Time history of *y*-axis plastic strain and stress in cell wall, cell strut edge, and cell strut middle at (*a*) the top surface and (*b*) bottom surface of the laser scanning path predicted by the cellular model (laser powder 5360 W, scanning speed 51.8 mm/s, and beam diameter 58 mm)

by the effective-property model (-2×10^5 Pa). This discrepancy is likely due to the fact that in the cellular model, calculated stress is stress of cell wall and cell strut of Al–Si alloy, and the magnitude of about $-(2.1\text{–}3) \times 10^6$ Pa is much small than the yield stress of Al–Si alloy, so no crush near the top surface is observed in simulated results. As indicated early, no crush was experimentally observed either. But in the effective-property model, the calculated stress is effective foam aluminum stress. So the magnitude is different.

As seen in Fig. 16(*b*), the points chosen are in the cell wall, edge of cell strut, and middle of cell strut at bottom surface. Contrary to the top surface, the plastic strain reaches a positive value at cell wall and cell strut middle, similar to that predicted by the effective-property model (Fig. 8), due to the little thermal expansion and the entirely compressive deformation at the top surface, tensile plastic strain occurs at cell wall and cell strut middle. And at cell strut edge, when the full tension of top surface initiates, compressive deformation occurred in the beginning, and because of size effect of the thinner beam at cell edge, compressive deformation becomes permanent plastic deformation. As to the stress, tensile stress is the main force at the bottom surface. And the magnitude of tensile stress at cell strut middle is the largest among cell wall, cell strut edge, and strut middle, so after 40–50 pass laser scanning, a crack initiates from strut middle, this is consistent with the experiment observation.

In addition, the cellular model involves more complex geometry and mesh and therefore is more computationally demanding, especially the mechanical model. Unless the inevitable heterogeneity of closed-cell foam aluminum including pore shape, size, and distribution is known and more precisely modeled, it appears that the effective-property model offers a better choice. Although the cellular model can explicitly predict foam's crush behavior, the stress/strain levels reached in laser forming do not normally reach the critical level for crush.

4.6 Effect of Foam Material. For the results reported above, Al–7%Si eutectic foam aluminum was used. The results were compared with Al–20%SiC foam aluminum. Both materials tested have similar density and closed-cell structure. They were cut into the same size ($100 \times 35 \times 11$ mm thick). For the Al–20%SiC foam aluminum, after 50 laser scans, bending angle was less than 1 deg, while for the Al–7%Si eutectic foam aluminum, bending angle reached about 16 deg. The thermal conductivity of two materials is similar. But the coefficient of thermal expansion of aluminum foams is reduced slightly by the addition of small amount of Si (7%), while it is significantly reduced by the addition of large amount of ceramic particles such as 20%SiC. As it is well known, the thermal expansion of material plays a very important role in thermal forming. This explains the significant difference in bending angle for the two foam aluminum materials with different compositions.

5 Conclusions

In this paper, the laser forming of Al–Si closed-cell foam plates was investigated through experiments and numerical simulations. An effective-property model and cellular model were constructed for the numerical investigation. The effective-property model predictions generally agree with experimental results of multiscan laser forming. Discrepancies under higher energy conditions were discussed. The cellular model somewhat underestimates the temperature gradients in the thickness direction but significantly overestimates the stress level likely due to the fact that the nonhomogeneity in pore shape, size, and distribution was inadequately accounted for.

Acknowledgment

The authors gratefully acknowledge Al–Si material from the Northeastern University, China.

The research is financially supported by the National Natural Science Foundation of China (51104110). Open fund from the State Key Laboratory of Advanced Processing and Recycling of Non-ferrous Metals (SKLAB02014006) is also appreciated.

References

[1] Fuganti, A., Lorenzi, L., Hanssen, A. G., and Langseth, M., 2000, “Aluminium Foam for Automotive Applications,” Adv. Eng. Mater., **4**(2), pp. 200–204.

[2] Guglielmotti, A., Quadrini, F., Squeo, E. A., and Tagliaferri, V., 2009, “Laser Bending of Aluminum Foam Sandwich Panels,” Adv. Eng. Mater., **11**(11), pp. 902–906.

[3] Quadrini, F., Guglielmotti, A., Squeo, E. A., and Tagliaferri, V., 2010, “Laser Forming of Open-Cell Aluminium Foams,” J. Mater. Process. Technol., **210**(11), pp. 1517–1522.

[4] Coquard, R., and Baillis, D., 2009, “Numerical Investigation of Conductive Heat Transfer in High-Porosity Foams,” Acta Mater., **57**(18), pp. 5466–5479.

[5] Santo, L., Guglielmotti, A., and Quadrini, F., 2010, “Formability of Open-Cell Aluminium Foams by Laser,” ASME Paper No. MSEC2010-34282, pp. 265–272.

[6] Quadrini, F., Bellisario, D., Ferrari, D., Santo, L., and Santarsiero, A., 2013, “Numerical Simulation of Laser Bending of Aluminum Foams,” Key Eng. Mater., **554–557**, pp. 1864–1871.

[7] Namba, Y., 1986, “Laser Forming in Space,” Proceedings of the International Conference on Lasers ‘85, Osaka, Japan, C. P. Wang, ed., STS Press, McLean, VA, Vol. 85, pp. 403–407.

[8] Geiger, M., and Vollertsen, F., 1993, “The Mechanisms of Laser Forming,” CIRP Ann., **42**(1), pp. 301–304.

[9] Ji, Z., and Wu, S., 1998, “FEM Simulation of the Temperature Field During the Laser Forming of Sheet Metal,” J. Mater. Process. Technol., **74**(1–3), pp. 89–95.

[10] Fang, X., Fan, Z., Ralph, B., Evansb, P., and Underhillc, R., 2003, “Effects of Tempering Temperature on Tensile and Hole Expansion Properties of a C-Mn Steel,” J. Mater. Process. Technol., **132**(1), pp. 215–218.

[11] Shen, H., Yao, Z. Q., Shi, Y. J., and Hu, J., 2007, “The Simulation of Temperature Field in the Laser Forming of Steel Plates,” Int. J. Modell. Identif. Control., **2**(3), pp. 241–249.

[12] Cheng, J., and Yao, Y. L., 2001, “Cooling Effects in Multiscan Laser Forming,” J. Manuf. Processes, **3**(1), pp. 60–72.

[13] Cheng, P., Yao, Y. L., Liu, C., Pratt, D., and Fan, Y., 2005, “Analysis and Prediction of Size Effect on Laser Forming of Sheet Metal,” SME J. Manuf. Processes, **7**(1), pp. 28–41.

[14] Bao, J., and Yao, Y. L., 2001, “Analysis and Prediction of Edge Effects in Laser Bending,” ASME J. Manuf. Sci. Eng., **123**(1), pp. 53–61.

[15] Li, W., and Yao, Y. L., 2001, “Laser Bending of Tubes: Mechanism, Analysis, and Prediction,” ASME J. Manuf. Sci. Eng., **123**(4), pp. 674–681.

[16] Li, W., and Yao, Y. L., 2000, “Numerical and Experimental Study of Strain Rate Effects in Laser Forming,” ASME J. Manuf. Sci. Eng., **122**(3), pp. 445–451.

[17] Shen, H., and Vollertsen, F., 2009, “Modelling of Laser Forming: An Review,” Comput. Mater. Sci., **46**(4), pp. 834–840.

[18] Mukarami, T., Tsumura, T., Ikeda, T., Nakajima, H., and Nakata, K., 2007, “Ansitropic Fusion Profile and Joint Strength of Lotus-Type Porous Magnesium by Laser Welding,” Mater. Sci. Eng. A, **456**(1–2), pp. 278–285.

[19] Yilbas, B. S., Akhtar, S. S., and Keles, O., 2013, “Laser Cutting of Aluminum Foam: Experimental and Model Studies,” ASME J. Manuf. Sci. Eng., **135**(5), p. 051018.

[20] Deshpande, V. S., and Fleck, N. A., 2000, “Isotropic Constitutive Models for Metallic Foams,” J. Mech. Phys. Solids, **48**(6–7), pp. 1253–1283.

[21] Yu, H. J., Yao, G. C., and Liu, Y. H., 2006, “Tensile Property of Al-Si Closed-Cell Aluminum Foam,” Trans. Nonferrous Met. Soc. China, **16**(6), pp. 1335–1340.

[22] Konstantinidis, I. Ch., Papadopoulos, D. P., Lefakis, H., and Tsipas, D. N., 2005, “Model for Determining Mechanical Properties of Aluminum Closed-Cell Foams,” Theor. Appl. Fract. Mech., **43**(2), pp. 157–167.